

Research Paper

Correspondence to:
Athanasios Ganas
aganas@noa.gr

DOI number:
<http://dx.doi.org/10.12681/bgsg.18070>

Keywords:
GNSS, Aegean,
displacement, earthquake,
scaling

Citation:
Athanasios Ganas,
Nikoletta Andritsou,
Chrysanthi Kosma,
Panagiotis Argyrakis,
Varvara Tsironi, George
Drakatos (2018), A 20-yr
database (1997-2017) of
co-seismic displacements
from GPS recordings in
the Aegean area and their
scaling with M_w and
epicentral distance. Bull.
Geological Society of
Greece, 52, 98-130.

Publication History:
Received: 19/07/2018
Accepted: 19/11/2018
Accepted article online:
20/11/2018

The Editor wishes to thank
Ricardo Caputo, Iannis
Koukouvelas and
Panagiotis Psimoulis for
their work with the
scientific reviewing of the
manuscript

©2018. The Authors
This is an open access
article under the terms of
the Creative Commons
Attribution License, which
permits use, distribution
and reproduction in any
medium, provided the
original work is properly
cited

A 20-YR DATABASE (1997-2017) OF CO-SEISMIC DISPLACEMENTS FROM GPS RECORDINGS IN THE AEGEAN AREA AND THEIR SCALING WITH M_w AND HYPOCENTRAL DISTANCE.

Athanasios Ganas^{1*}, Nikoletta Andritsou^{1,2}, Chrysanthi Kosma¹,
Panagiotis Argyrakis¹, Varvara Tsironi¹, George Drakatos¹

¹Institute of Geodynamics, National Observatory of Athens, 11810 Athens,
Greece aganas@noa.gr chrysanthi.kosma.varela@gmail.com pargyrak@noa.gr
barbara.tsir@gmail.com g.drakat@noa.gr

²National and Kapodistrian University of Athens, Department of Geology,
Athens, Greece nikandritsou@gmail.com

*corresponding author

Abstract

We describe and make available a dataset of 64 data points of Global Positioning System (GPS) displacements for significant, shallow earthquakes in Greece during the period 1997-2017. The displacement data can be used by earthquake geologists, engineers and seismologists in an effort to better understand the faulting process, the rupture mechanics, the pattern of ground-motions, and in engineering applications. We include recordings from GNSS networks at near-source to regional distances (2–132 km) for 11 earthquakes between global CMT moment magnitudes (M_w) 5.5 and 6.9. We also model the magnitude scaling properties of peak ground horizontal displacements (PGD and PGD-S) for these events using L1-norm minimisation regression. Our data indicate an almost linear attenuation of seismic strain with distance for this range of seismic magnitudes. We developed a set of relationships based on PGD (in cm) and distance to hypocentre R (in km), which may be used for the rapid estimation of the earthquake magnitude in near real-time.

$$M_w^{PGD} = [\text{LOG}(\text{PGD}) + 8.2849]/(1.6810 - 0.2453\text{LOG}R)$$

$$M_w^{PGD-S} = [\text{LOG}(\text{PGD-S}) + 8.0839]/(1.6793 - 0.2447\text{LOG}R)$$

Keywords: GNSS, Aegean, displacement, earthquake, scaling

Περίληψη

Στην παρούσα εργασία περιγράφουμε και διαθέτουμε μία βάση εξήντα τεσσάρων (64) σεισμικών μετατοπίσεων από τις καταγραφές μόνιμων σταθμών GPS, κατά την εικοσαετή χρονική περίοδο 1997-2017. Οι μετατοπίσεις οφείλονται σε μεγάλους, επιφανειακούς σεισμούς στον Ελληνικό χώρο οι οποίοι προκάλεσαν επιφανειακές κινήσεις (της τάξεως χιλιοστών έως δεκάδων εκατοστών) ανιχνεύσιμες από δίκτυα GPS-GNSS. Στην βάση περιλαμβάνονται δεδομένα μόνιμης μετατόπισης για αποστάσεις μεταξύ 2-132 km από το υπόκεντρο και για 11 σεισμούς με μεγέθη ροπής μεταξύ $5.5 \leq M_w \leq 6.9$. Αυτά τα δεδομένα είναι χρήσιμα σε γεωλόγους, σεισμολόγους και μηχανικούς επειδή συμβάλουν στην πληρέστερη κατανόηση της μηχανικής των διαρρήξεων, της κατανομής των επιφανειακών παραμορφώσεων μετά από μεγάλους σεισμούς αλλά και σε άλλες εφαρμογές σεισμικής μηχανικής. Επιπλέον, έγινε ανάλυση με πρώτη νόρμα (*L1-norm*) παλινδρόμησης της απόσβεσης της μόνιμης, οριζόντιας επιφανειακής μετατόπισης συναρτήσει του μεγέθους και υποκεντρικής απόστασης. Βρήκαμε ότι τα δεδομένα μας ταιριάζουν καλύτερα με μία γραμμική συμπεριφορά για αυτό το εύρος μεγεθών. Προτείνουμε δύο εμπειρικές σχέσεις για τον υπολογισμό του σεισμικού μεγέθους βάσει της εδαφικής μετατόπισης και της απόστασεως από το υπόκεντρο, οι οποίες μπορούν να χρησιμοποιηθούν εφόσον είναι διαθέσιμες επιλύσεις σταθμών σε σχεδόν-πραγματικό χρόνο.

Λέξεις κλειδιά: GNSS, Αιγαίο, μετατόπιση, σεισμός, συσχέτιση

1. Introduction

1.1 GNSS data for ground displacements

Over the last twenty (20) years, displacements from Global Navigation Satellite System (GNSS) data, specifically from Global Positioning System (GPS) have become a useful measurement in seismology and earthquake geology. Such data have been used to quantify the intensity of ground deformation following strong earthquakes, to infer the geometry and kinematics of the seismic fault in case of “blind” ruptures as well as to contribute to fault inversion models (Ganas et al., 2009; 2013; 2016; Hreinsdottir et al. 2009; Devoti et al. 2012; Saltogianni et al.,

2015; Briole et al. 2015; Chousianitis et al., 2016; Avallone et al., 2017; Melgar et al., 2017; Howell et al., 2017; Chousianitis, and Konca, 2018).

The GNSS technique relies on precise measurements of electromagnetic waves between a GNSS antenna and a constellation of satellites with precisely known orbits. Geodetic analysis of the dual-frequency GNSS data results in reliable and unsaturated measurements of ground motion displacement (e.g. Melgar et al., 2015; Geng et al., 2016; 2017). GNSS directly measures displacements in an absolute global reference frame (ITRF 2008 and so on), but rigorous post-processing of the data is necessary to measure offsets at the sub-millimetric level. Thus, the space observations are useful for extracting ground displacements following moderate to large events ($5 \leq M \leq 9$) as it has been demonstrated in many cases (see Melgar et al., 2015 and Ruhl et al. 2017, 2018, for a summary of recent literature).

Accordingly, GNSS technology is widely used in earthquake source studies where it is usually inverted on its own, or jointly with other geophysical data sets (e.g. InSAR, seismology), to image the kinematic source process of $M6+$ events (Huang et al. 2013; Chousianitis et al., 2016; Melgar et al., 2017; Avallone et al., 2017). High-rate GNSS has also been employed in studies of long-period ground motions, and in structural monitoring (Moschas and Stiros, 2011; 2014). The latest application of GNSS is the incorporation of the geodetic component in earthquake early warning systems (e.g. Murray et al., 2018). A review of the evolution, uses, and algorithms behind GNSS can be found in Bock and Melgar (2016).

1.2 NOANET and other GNSS networks

In Greece NOA operates a national GNSS network, NOANET (Ganas et al., 2008; 2011; 2012; 2013a; Chousianitis et al., 2013) under an open data policy. Thus, it is possible to access the data after a seismic event. The GNSS data are collected in a centralized repository and they are accessible via the NOA GSAC tool (Argyris et al., 2016). All stations are equipped with dual-frequency GPS receivers.

The first installation of NOANET was completed on February 12, 2006 in the island of Cephalonia, Ionian Sea (Fig. 1). This site is co-located with the NOA seismological station VLS and had been tested for several months during 2005 using a Leica 1200 receiver provided by Joel VandenBroek of Leica-Geosystems SA. A similar test was synchronously performed in another co-located station, RLSO in NW Peloponnese (using geodetic equipment provided by Evangelos Lagios, NKUA; operated until 9 March 2009 under the code RLS_). In both localities, GPS signal quality was excellent. Station NOA1 was installed on March 13, 2006; it is serviced by a Leica 1200GRX receiver and a AT 504 Choke-ring antenna. Then, given the limited amount of resources available to us during the period 2007-2015, we focused in high seismic hazard regions such as western Greece - south Peloponnese and in the central-northern Aegean, respectively. Stations VLSM, KIPO, PONT and SPAN are aligned along the Cephalonia Transform Fault (CTF), a large dextral transcurrent fault zone associated with strong, shallow earthquakes. The 140-km long, right-lateral CTF accommodates the relative motion of the Apulia (Africa) and Aegean (Eurasia) lithospheric plates with a 70-85 km cumulative dextral displacement (Pearce et al., 2012). Stations PONT and SPAN are located on the island of Lefkada at about 7 km to the east of CTF. Station KASI is located in northern Corfu island at about 30 km to the east of the Apulian thrust, a rather unexplored active structure which may be associated with large historical earthquakes (e.g. Nappi et al., 2017). Stations PRKV, SKYR and LEMN are located near to the North Anatolian Fault (NAF) branches in the North Aegean Sea. Most stations are co-located with broadband seismometers and/or strong motion instruments. All above stations provided excellent data after strong, shallow earthquakes in Greece since 2008.

In this paper we describe and make open a database of GNSS displacement data that various authors have published over the last 20 years in the broader Aegean region. The earthquakes that caused the ground deformation are listed in Table 1. The displacements database consists of 64 two-component GNSS recordings of ground motion, rigorously processed in standard geodetic approaches including by point positioning algorithms (PPP; for example, Lefkada 2015 M6.5 event; Ganas et al., 2016; Avallone et al. 2017) or double-difference approach (as the RLSO station during the 2008 Kato Achaia M6.5 earthquake,

Ganas et al., 2009) to obtain displacements in geodetic coordinates. The displacement data are presented in a unified text format in supplementary material (**Table S1**). The number of recordings per station is shown in **Supplementary Figure S1**.

Table 1. Focal parameters of strong and shallow Greek earthquakes used in this study, period 1997-2017. Data for individual events are referenced in the last column. Moment magnitude is determined after <http://www.globalcmt.org/>. Location of events is shown in Fig. 1.

Event Number	Date	Latitude	Longitude	Depth (km)	Mw (GCMT)	Reference
1	19971118	37.4800	20.6900	10.0	6.6	ISC Event 1053117
2	20010726	39.0500	24.3500	19.0	6.4	NOA catalogue
3	20030814	38.8300	20.6400	6.8	6.2	Ilieva et al. 2016
4	20080608	37.9400	21.4780	18.0	6.4	Ganas et al. 2009
5	20100118	38.3962	21.9039	8.5	5.5	Ganas et al. 2013
6	20100122	38.4075	21.9422	5.1	5.4	Ganas et al. 2013
7	20140126	38.2102	20.4614	16.5	6.1	Karastathis et al. 2015
8	20140203	38.2734	20.4310	4.6	6.0	Karastathis et al. 2015
9	20140524	40.2900	25.4000	14.0	6.9	NOA MT event page
10	20151117	38.6755	20.5930	9.6	6.5	Ganas et al. 2016
11	20170720	36.9553	27.4484	9.2	6.6	Ganas et al. in review

In addition, this type of data is useful to remove offsets of tectonic origin from GNSS time-series so the station velocity can be used in tectonic geodesy studies (e.g. Avallone et al., 2004; Reilinger et al., 2006; Rontogianni, 2010; Ganas et al., 2013a; Chousianitis et al., 2015; Marinou et al., 2015; Sakkas and Lagios, 2017). As a demonstration of the utility of the database for earthquake source studies, we applied regression analysis to obtain peak ground displacement (PGD) scaling relationships, following the procedures provided by Crowell et al. (2013, 2016) and Melgar et al. (2015). This analysis also helps to understand the attenuation pattern of seismic strain immediately following strong earthquakes.

The events range in magnitude from $M_w=5.5$ (2010 Efpalio; Ganas et al., 2013b) to $M_w=6.9$ (2014 Samothraki; Saltogianni et al., 2015; Kiratzi et al., 2016). The database includes continental strike-slip (e.g. 2008 $M_w=6.5$ in NW Peloponnese; Ganas et al., 2009), intraplate normal (e.g. 2010 $M_w=5.5$ Efpalio) and Hellenic subduction zone events (1997 Strofades; Hollenstein et al., 2006).

All events have hypocentres shallower than 30 km and the number of stations available for each event varies widely (Table 2). Some have only a few sites, such as the 1997 $M_w=6.6$ Strofades earthquake on the Hellenic megathrust or the $M_w=6.4$ 2001 Skyros earthquake which have only two stations with data. More recent events, like the $M_w=6.9$ 2014 Samothraki earthquake and the Kos 2017 $M_w=6.6$ earthquake have 15 and 18 records, respectively. As GNSS data are noisy, some of the stations in operation during moderate magnitude events, but located far from the source, did not record any meaningful signals. We use the global CMT moment magnitude database for our scaling tests since it has been available long before the rise of the GNSS era (late 80s).

Table 2. List of strong and shallow Greek earthquakes with published GPS offsets, period 1997-2017. The horizontal offsets are combined into a peak ground displacement (PGD) as defined in equation 1 below. Column stations denotes the number of permanent GNSS stations with available recordings. Location of events is shown in Fig. 1.

Event No	Event Name	Source of GPS offsets	Stations	RGD range (cm)
1	Strofades Eq 1997	Hollestein et al., 2006	2	1.40-6.45
2	Skyros Eq 2001	Hollestein et al., 2008	2	2.60-4.15
3	Lefkada Eq 2003	Hollestein et al., 2008	10	0.10-4.50
4	SW-Achaia Eq 2008	Ganas et al., 2009	1	0.35
4	SW-Achaia Eq 2008	Gianniou, 2011	2	0.50-0.55
5	Efpalio Eq 2010-01-18	Ganas, et al., 2013	1	0.48
6	Efpalio Eq 2010-01-22	Ganas, et al., 2013	1	0.24
7	Cephalonia Eq 2014-01-26	Ganas et al., 2015	5	0.08-3.60
8	Cephalonia Eq 2014-02-03	Ganas et al., 2015	3	0.09-1.23
9	North Aegean Sea Eq 2014	Ganas et al., 2014, unpublished report	4	1.31-3.51
9	North Aegean Sea Eq 2014	Saltogianni et al., 2015	11	0.24-6.45
10	Lefkada Eq 2015	Ganas et al., 2016	4	0.05-27.80
11	Kos Eq 2017	Ganas et al., in review	18	0.20-9.90

The data comprise GPS static offsets (measured on the horizontal components, North-South and East-West) regarding the following earthquakes (Table 2): 1997 Strofades M6.6 (Hollenstein et al., 2006), 2001 Skyros M6.4 (Hollenstein et al. 2008), 2003 Lefkada M6.3 (Hollenstein et al. 2008), 2008 Kato Achaia M6.5 (Ganas et al., 2009; Gianniou, 2011), 2010 Efpalio M5.5 (Ganas et al. 2013b), 2014 Cephalonia M6.1-M6.0 (Ganas et al., 2015), 2014 Samothraki M6.9 (Saltogianni et al, 2015), 2015 Lefkada M6.5 (Ganas et al., 2016), and 2017 Kos M6.6 (Ganas et al. in review). The offsets on the vertical component were not retrievable in most cases or were within the level of GPS noise, so this component was ignored in further analysis.

The displacement data are structured as follows (Table S1). There are several records per event clearly labelled with event names. For each event important metadata are reported (date, magnitude) as well the GPS site (network code) that provided co-seismic offsets. There are two columns which contain static offsets named PGD (*Peak ground displacement*) and PGD-S (*PGD-squared*) offsets, respectively. PGD/PGD-S are defined as in equations (1) and (2) respectively. M_w is the known moment magnitude for the earthquake from the global centroid moment tensor (CMT) catalog (<http://www.globalcmt.org/>), and R is the hypocentre- to-station distance calculated on a spherical Earth.

For each station-event pair, we compute the hypocentral distance R , using either the manual location by NOA (<http://www.gein.noa.gr/en/seismicity/earthquake-catalogs>) or relocated data when available (Table 1; for example for event #1 location is from ISC; event #3 location is from Ilieva et al., 2016; events #7 and #8 locations are from Karastathis et al. 2015) as we seek to minimize location error in our regression analysis. We chose to work with hypocentral distance because our station coverage is relatively dense so many stations are located at distances < 25 km for the epicentre (about 1/3 of our data) so the depth factor becomes important for regression. Furthermore, many local GNSS networks are expanding in Greece (under the framework of project HELPOS) so more near-field data will become available and our equations can be used readily in order to estimate moment magnitudes.

2.2 GNSS data quality

The quality of the GNSS data (in short QC) obtained by the NOA receivers is monitored routinely. Our QC analysis examines the daily, 30-second RINEX data file for each NOANET receiver focusing primarily on multipath effects. The multipath error describes the reflections of the GNSS satellite signals that come back to the antenna and it is mainly produced from surfaces in the vicinity of the antenna such as iron, water, glass etc. The signals arrive to the antenna through two different paths which causes delaying compared to the direct path. Delaying introduces errors in pseudorange and carrier phase measurements. To examine the level of multipath error of the GNSS stations during the day of the earthquakes we use TEQC (Estey and Meertens, 1999) to process RINEX (Receiver Independent Exchange Format) files. Quality control with TEQC produces files of satellite azimuth, satellite elevation, multipath at L1 (1575.42 MHz) and multipath at L2 (1227.60 MHz) frequencies, also signal to noise ratio of L1, L2 if data exist, in COMPACT2 format.

Then, we modified the *GNU-qcplot* software <http://www.gnuplot.info/> to produce skyplots and receiver plots of stations that recorded the co-seismic offsets (Fig. 2 and Fig. 3). A skyplot is a simple illustration of GPS satellite trajectories over a given GPS site (Marshall, 2002; Hilla, 2004). These plots, also called satellite visibility diagrams, provide an intuitive feel for satellite geometry and they reveal the impact of obstructions on satellite visibility, as well as they display where the positive and negative values of pseudorange multipath are plotted with respect to each satellite's azimuth and elevation (Fig. 2, Fig. 3). The *Qcplot* software process the TEQC outputs and produces a file from combination of azimuth and elevation with respect to multipath files of L1 and L2. With the use of skyplots it is easy to identify and eliminate if possible the source of multipath around the antenna and produce high quality RINEX files. In our examined dates (see Table 1) we confirm that the data (GPS observations) used in further processing are free of multipath effects. The only exceptions include a) for the 17 November 2015 earthquake station PONT in L1 (Figure 2a; but not in L2; see Fig. 3a) there is multipath at 3 satellites at azimuth N150°E at 15° elevation b) for the 8 June 2008 earthquake at station RLS_L2 (Riolos; new code is RLSO) there is multipath that affects 4 satellites at azimuth N330°E around 20° elevation (Fig. 2b).

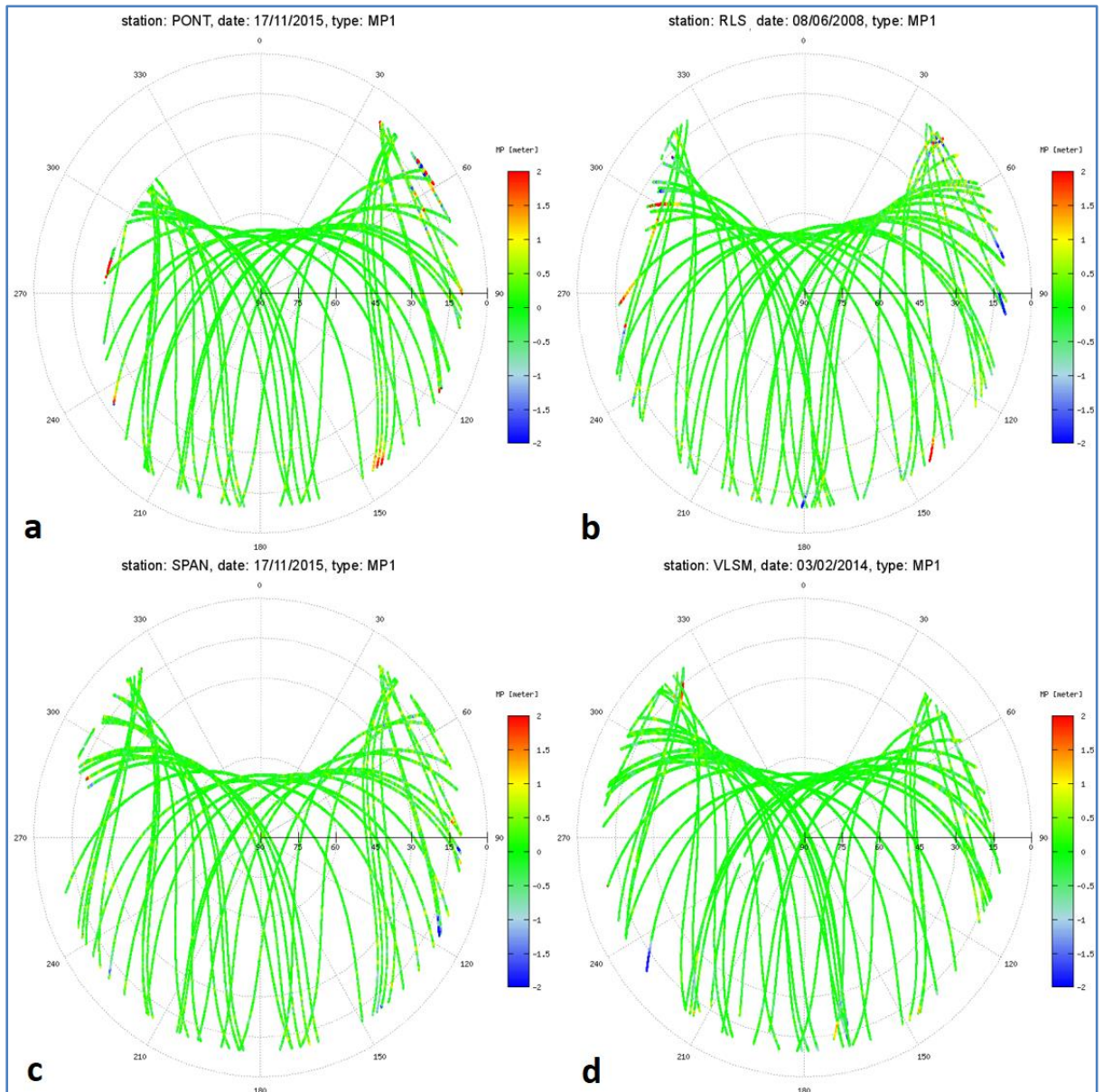


Fig. 2: Skyplots showing L1 multipath effects for four NOA stations that recorded co-seismic offsets. Event dates are shown beneath each plot. The daily rinex file was processed: a) PONT b) RLS_ c) SPAN and d) VLISM. Elevation cut-off angle is 10° . Colour scale is in m. [see online supplementary material for higher resolution of this figure].

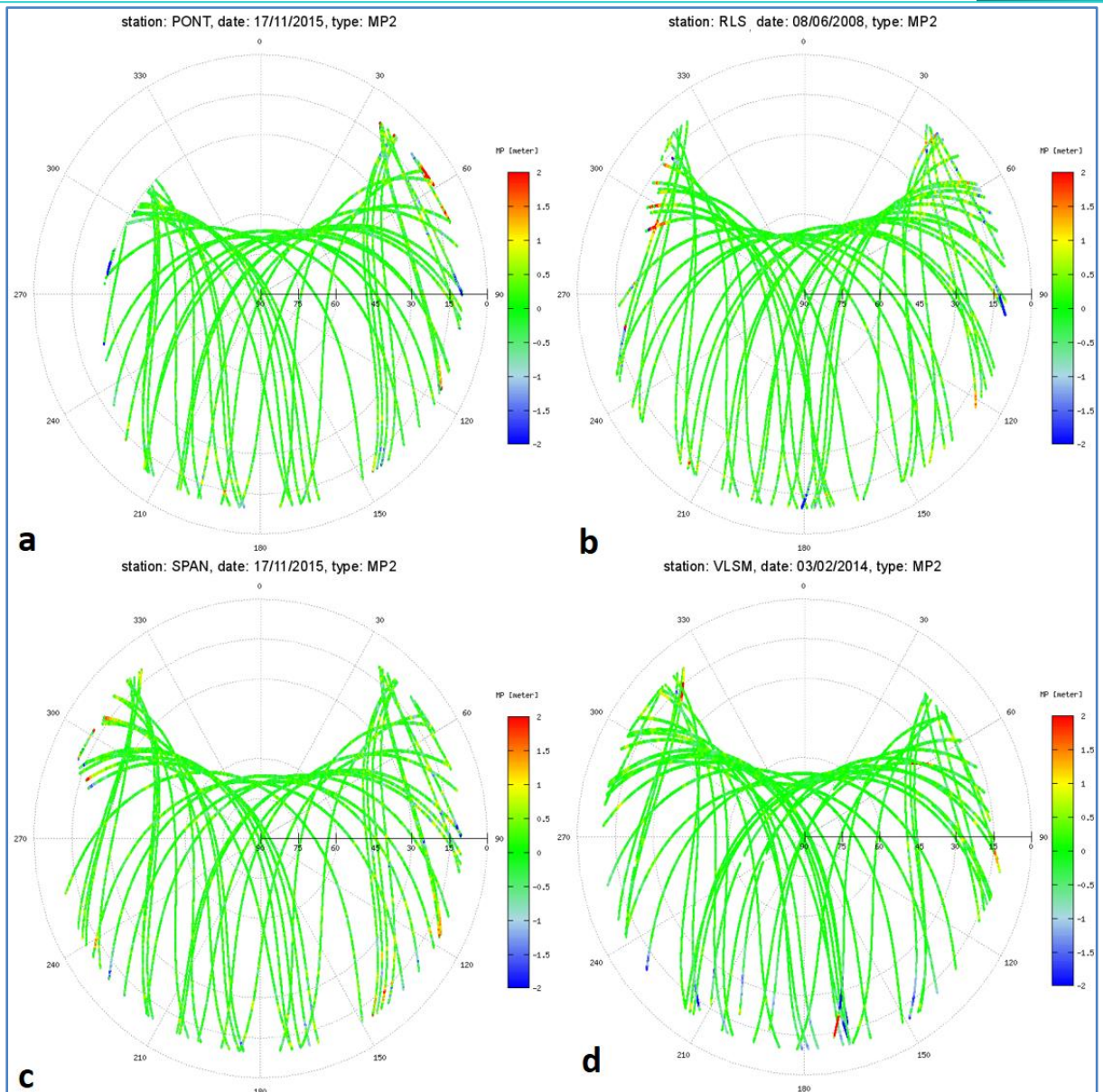


Fig. 3: Skyplots showing L2 multipath effects for four NOA stations that recorded co-seismic offsets. Event dates are shown beneath each plot. The daily rinex file was processed: a) PONT b) RLS_ c) SPAN and d) VLISM. Elevation cut-off angle is 10° . Colour scale is in m. [see online supplementary material for higher resolution of this figure].

3. Discussion

3.1 PGD scaling relationship for Aegean earthquakes

Melgar et al. (2015) and Ruhl et al. (2018) produced PGD scaling laws and proposed algorithms for their real-time use as an unsaturated estimator of earthquake magnitude. In this study we use only horizontal offsets to investigate

their usefulness in the magnitude range $5.5 \leq M \leq 6.9$, which most frequently occurs in the Aegean region. The complete database includes 11 events during the period 1997-2017 (see Fig. 1 for locations). We consider those published offsets as mostly co-seismic because they originate from averaged positions of a few days following the mainshock although we are aware that a small post-seismic contribution maybe present in the data. For example, comparable events to the Aegean ones examined here like the 2003 M6.5 San Simeon earthquake were followed by postseismic moment release of 14% w.r.t that of the mainshock (Johanson and Bürgmann, 2010).

We used the A_{N-S} and A_{E-W} components of ground displacement (A stands for amplitude), North-South and East-West direction, respectively. Then, we calculated the quantities PGD (*Peak Ground Displacement*) and PGD-S (*Peak Ground Displacement - Squared*) as follows:

$$PGD = (|A_{N-S}| + |A_{E-W}|)/2 \quad (1)$$

$$PGD-S = (A_{N-S}^2 + A_{E-W}^2)^{1/2} \quad (2)$$

So PGD is the mean value of the absolute horizontal displacement in two orthogonal directions (in cm), while PGD-S is the resultant horizontal displacement (in cm). We want to estimate a relation of the type:

$$\text{LOG}(x) = \mathbf{A} + \mathbf{B} * M_w + \mathbf{C} * M_w * \text{LOGR} \quad (3)$$

where x is either PGD or PGD-S, M_w is the magnitude of the earthquake event and R is the hypocentral distance of the GPS station to the earthquake's epicenter (see Table S1 for data).

We use L1-norm minimization regression to correlate M_w and LOGR with PGD (Fig. 4) and PGD-S (Fig. 5). This regression is a least squares method with a penalty of the L1-norm form multiplied by a factor λ . Using the *lasso* command in MATLAB with $y = \text{LOG}(PGD)$ or $y' = \text{LOG}(PGD-S)$, $x_1 = M_w$ and $x_2 = M_w \text{LOG}(R)$ we obtain sets of the coefficients \mathbf{A} , \mathbf{B} and \mathbf{C} for different values for λ . We applied 6-fold validation to our results and selected the set \mathbf{A} , \mathbf{B} , \mathbf{C} for the

λ factor that minimized the MSE (Mean Square Error). The regression values are given in Table 3.

The regression for PGD-S minimizes the Mean Square Error in comparison to PGD, so we expect it to show a better fit. The best example of PGD scaling over a 10-100 km hypocentral distances is presented by the Kos 2017 earthquake data (red rhomb symbol; Fig. 4 and Fig. 5).

In Fig. 4 & 5 we plot the GNSS displacement data as in colour scale from blue to red based on the real magnitude of the earthquakes (so the data corresponding to the highest magnitude M6.9 are shown in dark red).

Table 3. Results of regression performed in MATLAB software.

Regression Target	λ	min MSE (Mean Square Error)	A	B	C
PGD	0.0000217	0.1209	-8.2849	1.6810	-0.2453
PGD-S	0.0000216	0.1193	-8.0839	1.6793	-0.2447

So, using the values of Table 3 equation (3) becomes:

$$\text{LOG(PGD)} = -8.2849 + 1.6810 * M_w - 0.2453 * M_w * \text{LOGR} \quad (4)$$

$$\text{and LOG(PGD-S)} = -8.0839 + 1.6793 * M_w - 0.2447 * M_w * \text{LOGR} \quad (5)$$

For the parameters A, B and C of the two relationships are also reported the corresponding values from the var-covariance matrix (Table 4 for PGD and Table 5 for PGD-S, respectively). The derivation of the var-covariance matrix is presented in the **Supplementary Text S1** (at the end of this paper).

Table 4. The covariance matrix for the A, B, C coefficients calculated using PGD (equation 4).

PGD	A	B	C
A	4.2659	-0.8515	0.1188
B	-0.8515	0.1700	-0.0237
C	0.1188	-0.0237	0.0033

Table 5. The covariance matrix for the A, B, C coefficients calculated using PGD-S (equation 5).

PGD-S	A	B	C
A	4.2337	-0.8450	0.1178
B	-0.8450	0.1687	-0.0235
C	0.1178	-0.0235	0.0033

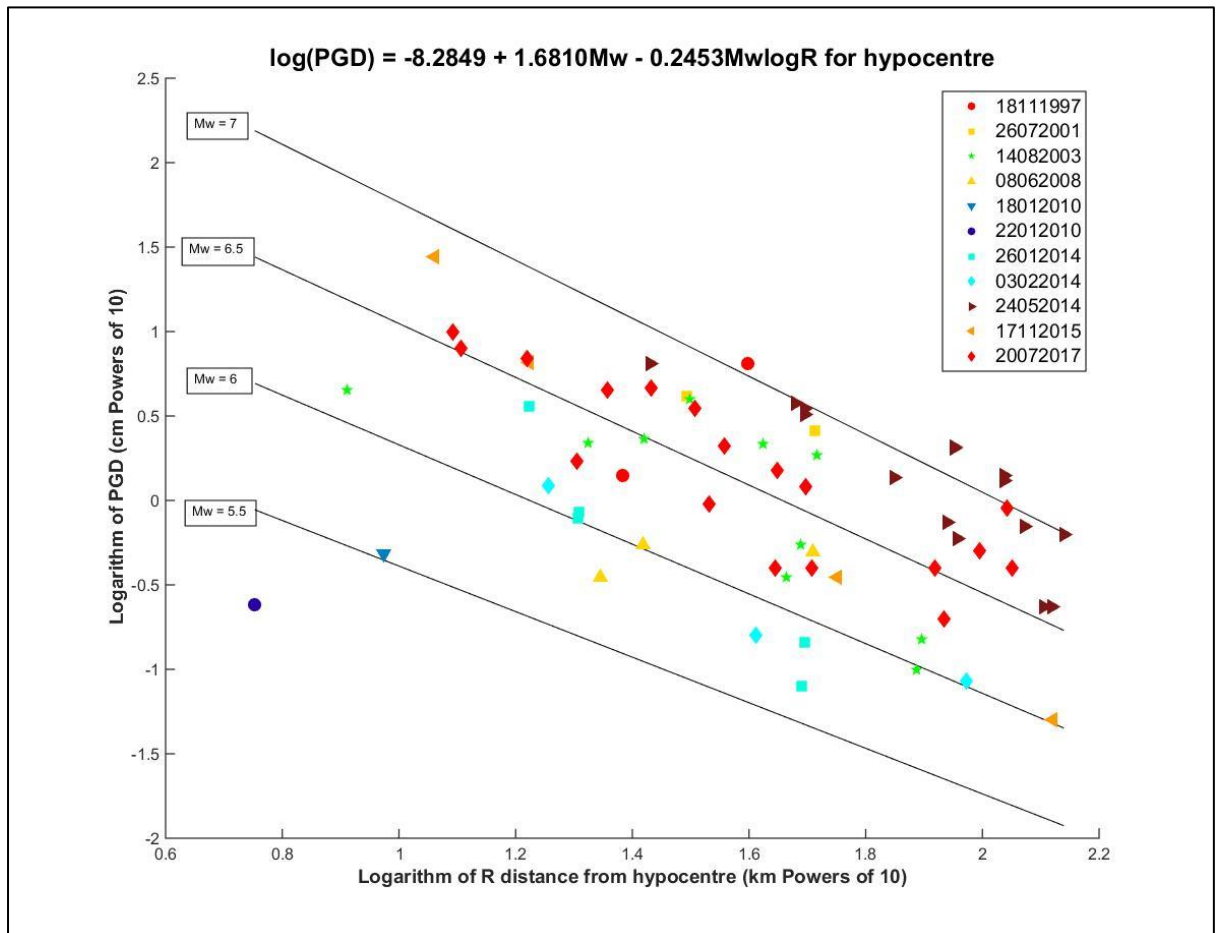


Fig. 4: Scatter plot in log-log space showing decrease of PGD (cm) with hypocentral distance (km) in the magnitude range 5.5-6.9 (11 events from the Aegean area, period 1997-2017). Date format in legend (upper right) is DDMMYYYY. The oblique black lines are the predicted scaling values for a particular earthquake magnitude from the L1 regression of the PGD measurements. PGD is defined in (1). The PGD colour scale ranges from blue to red based on the real magnitude of the earthquakes (so the data corresponding to the highest magnitude M6.9 are shown in dark red).

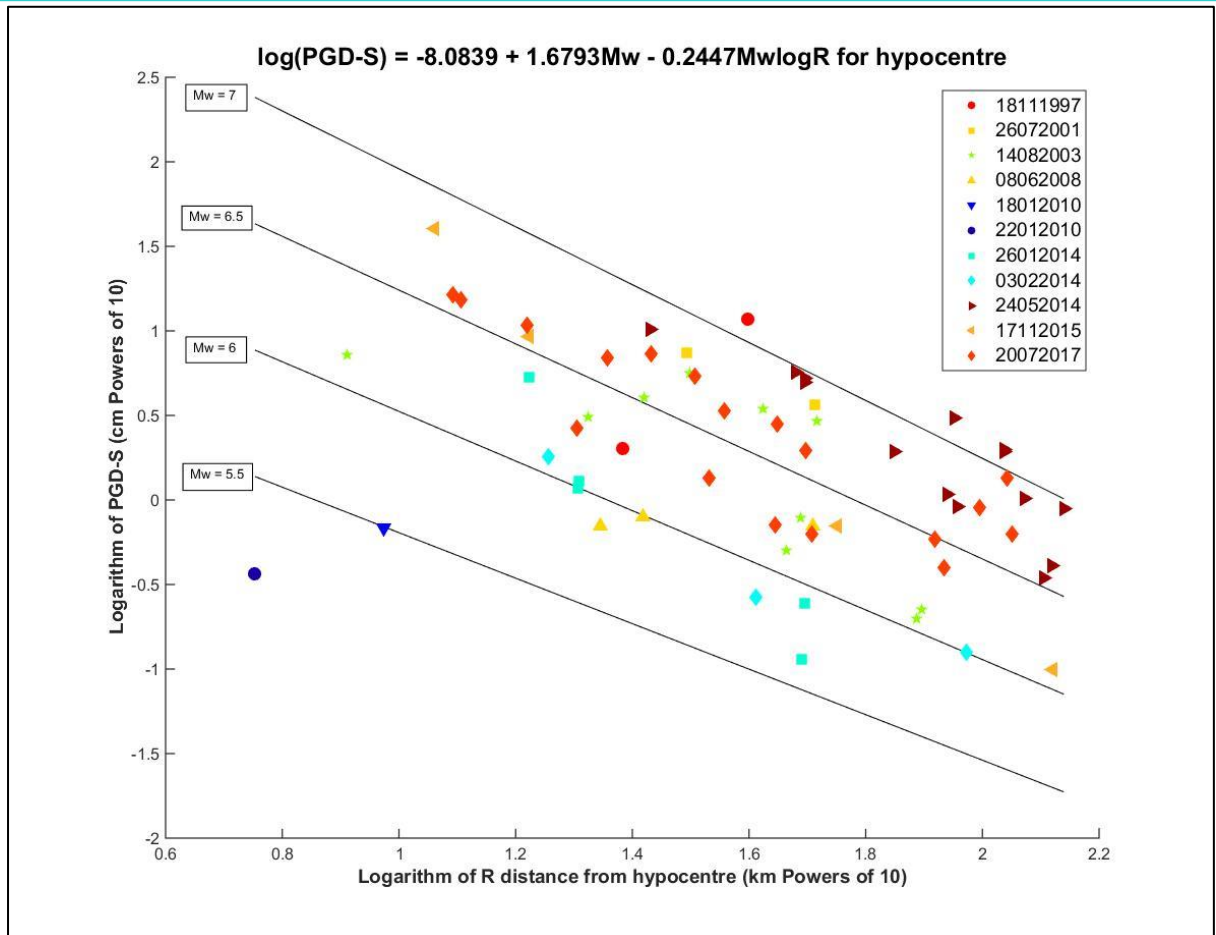


Fig. 5: Scatter plot in log-log space showing decrease of PGD-S (cm) with hypocentral distance (km) in the magnitude range 5.5-6.9. Date format in legend (upper right) is DDMMYYYY. The oblique black lines are the predicted M_w scaling values from the L1 regression of the PGD-S measurements. PGD-S is defined in (2).

3.2 GNSS magnitude (estimated) vs real Magnitude

The paper focuses on the derivation of a relationship between the Peak Ground Displacement (PGD & PGD-S), as it is defined by GNSS (GPS) measurements, and the moment magnitude (M_w) of the earthquake. The main aim is to develop a set of relationships based on eleven (11) earthquake cases in Greece, which may be used for the rapid estimation of the earthquake magnitude in near real-time. As such it would be useful to produce a comparison table for those 11 events, with the real magnitude (M_w) and the GNSS-estimated one (M_{GNSS} ; as the average of the estimates of the corresponding earthquake including the uncertainty range). This might not be representative for earthquakes with very

few stations (for example the 2010 Efpalion events or the 1997 event offshore Strofades; see Table 2) but still it will draw more easily the final conclusions.

For every seismic event i we had N_i values for M_w . We calculated the mean estimated values $M_{wi}^{PGD}_{mean}$ and $M_{wi}^{PGD-S}_{mean}$, the standard errors s^{PGD} and s^{PGD-S} and the differences $\Delta M^{PGD} = M_{wi} - M_{wi}^{PGD}_{mean}$ and $\Delta M^{PGD-S} = M_{wi} - M_{wi}^{PGD-S}_{mean}$. The results of this analysis are presented in Table 6 (for PGD) and Table 7 (for PGD-S) for the data set of the 64 points. We calculated the standard deviation for our GNSS estimated magnitudes (M_w or M_{GNSS}) for each seismic event for PGD and PGD-S approach. For events with several data points (for example events #3, #9, #11) the standard deviation of estimated magnitudes is less than 0.3 units.

We then solved the LOG(PGD) and LOG(PGD-S) relations for M_w .

We got:

$$M_w^{PGD} = [\text{LOG}(\text{PGD}) + 8.2849]/(1.6810 - 0.2453\text{LOG}R) \quad (6)$$

$$M_w^{PGD-S} = [\text{LOG}(\text{PGD-S}) + 8.0839]/(1.6793 - 0.2447\text{LOG}R) \quad (7)$$

Where PGD and PGD-S are in cm and R in km, respectively.

In 7 events the magnitude difference (ΔM) $M_w - M_{GNSS}$ is less than or equal to 0.1 units using the PGD approach (this is true for 6 events using the PGD-S approach). The largest deviation is observed in the case of event 4 (the 2008 M6.4 earthquake in NW Peloponnese) where the estimated magnitude from GNSS is 5.88 (PGD relationship) or 5.87 (PGD-S relationship), i.e. it is underestimated by 0.5 units of magnitude. The reason for this underestimation is the relatively large depth of mainshock (18 km; Ganas et al., 2009) and the thick pile of sedimentary rocks in NW Peloponnese (including several km of Triassic evaporites; Serpetsidaki et al. 2014) that resulted in significant attenuation of the released elastic strain energy. The second larger deviation concerns the 2001 Skyros strike-slip earthquake where the GNSS-estimated magnitude is larger than the M_w by 0.44 units of magnitude. Here, we believe that the GNSS offsets may have been overestimated by the analysts.

Table 6. GNSS-estimated magnitude ($M_{wi}^{PGD_{mean}}$) vs real magnitude using the PGD relationship (6). s^{PGD} is the standard deviation and ΔM is calculated as $\Delta M^{PGD} = M_w - M_{wi}^{PGD_{mean}}$.

Event Number	Date	No of stations	Estimated Magnitude $M_{wi}^{PGD_{mean}}$	Standard Deviation s^{PGD}	Mw (GCMT)	ΔM
1	19971118	2	6.67	0.55	6.6	-0.07
2	20010726	2	6.84	0.09	6.4	-0.44
3	20030814	10	6.39	0.29	6.2	-0.19
4	20080608	3	5.88	0.27	6.4	0.52
5	20100118	1	5.52	-	5.5	-0.02
6	20100122	1	5.12	-	5.4	0.28
7	20140126	5	6.00	0.26	6.1	0.10
8	20140203	3	5.98	0.14	6	0.02
9	20140524	15	6.92	0.19	6.9	-0.02
10	20151117	4	6.43	0.37	6.5	0.07
11	20170720	18	6.55	0.21	6.6	0.05

Table 7. GNSS-estimated magnitude vs real magnitude using the PGD-S relationship (7).

Event Number	Date	No of stations	Estimated Magnitude	Standard Deviation	Mw (GCMT)	ΔM
1	19971118	2	6.68	0.60	6.6	-0.08
2	20010726	2	6.84	0.03	6.4	-0.44
3	20030814	10	6.38	0.29	6.2	-0.18
4	20080608	3	5.87	0.21	6.4	0.53
5	20100118	1	5.49	-	5.5	0.01
6	20100122	1	5.12	-	5.4	0.28
7	20140126	5	5.99	0.27	6.1	0.11
8	20140203	3	5.97	0.12	6	0.03
9	20140524	15	6.90	0.18	6.9	0.00
10	20151117	4	6.46	0.31	6.5	0.04
11	20170720	18	6.56	0.21	6.6	0.04

While the good fit of our GNSS-estimated magnitude vs. the real magnitude determined from moment tensor inversion is expected given the training dataset of Table S1 we investigated further the applicability of our empirical relationships (equations 6 & 7) using an independent dataset of GNSS co-seismic displacements. We used the co-seismic offsets of the 2018 October 25, 22:54 UTC megathrust earthquake offshore Zakynthos (Ionian Sea, Greece; <https://earthquake.usgs.gov/earthquakes/eventpage/us1000hbb1/executive>) at nine (9) stations that were provided to us by Pierre Briole (ENS, Paris; table 8).

To perform the validation, we used the NOA catalogue epicentre (37.3410° North - 20.5123° East), the NOA depth (9.9 km) and the GCMT $M_w=6.8$ (the NOA $M_w=6.7$). We obtained a GNSS magnitude = 6.73 which was derived as a mean value of all 9 data points (stations and distances in Table 8). Our estimate differs by an amount of 0.03 magnitude units from the NOA moment magnitude estimation and by 0.07 magnitude units from USGS & GCMT moment magnitudes. We note that this encouraging result is due to the availability of co-seismic offsets from nine (9) stations, however the magnitude variability ranged from 5.8-5.9 (VLSM) to 7.0-7.1 (ZAKU and ZAKY). This is a clear message that single-station estimates may be risky in real-time applications of this method.

Table 8. Estimation of earthquake magnitude for the 2018 Zakynthos earthquake using the GNSS data. PGD/PGD-S is in cm, R is in km. The magnitudes were calculated using the empirical relationships of equation 6 (PGD) and equation 7 (PGD-S).

PGD	R	PGD-S	M_w PGD	M_w PGD-S	Station
1.30	90.410	1.89	6.99	6.96	AMAL
0.25	135.058	0.36	6.63	6.60	TROP
3.40	59.771	4.91	7.08	7.05	ZAKU
3.30	59.420	4.74	7.07	7.03	ZAKY
1.20	92.345	1.79	6.98	6.96	PYRG
0.25	116.036	0.41	6.54	6.56	KOPA
3.50	46.582	5.15	6.94	6.92	STRF
0.05	93.727	0.10	5.83	5.92	VLSM
0.25	115.525	0.41	6.54	6.55	PYLO
			6.73		mean M_w PGD
				6.73	mean M_w PGD-S

3.3 Scaling implications for seismic strain attenuation

Our results indicate almost linear scaling of PGD/PGD-S with hypocentral distance and earthquake magnitude (M_w), or that seismic strain attenuation scales linearly with earthquake magnitude and distance from hypocentre. It is impressive that for elastic strains the GNSS technology can map earthquake-induced deformation at 100 km distance from the hypocentre, that is up to 4-5 fault lengths for magnitude M_6+ events. This indicates that at such short time-

scales the earth's upper crust is 100% coupled and it behaves as an almost perfect elastic body.

In addition, this empirical scaling approach seems to hold irrespective of the mechanism of the earthquake, although more data are needed to support this statement. Our Aegean dataset is dominated by strike-slip events (7 out of 11) while normal-slip events (3 out of 11) and reverse-slip (1 out of 11) are under-represented. We note that our successful validation (Table 8) was conducted on the 2018 Zakynthos megathrust event. The inclusion of more dip-slip events in our database may also necessitate the future incorporation of the Up-component in our PGD (as in Ruhl et al., 2018) as ruptures along inclined planes create significant vertical deformation which is asymmetric (i.e. King et al., 1988; Atzori et al. 2008; Cheloni et al. 2014; Ganas et al, 2018).

The observed PGD- M_w -R scaling also implies that the gradient of the co-seismic displacement (and hence the efficiency of seismic radiation in inducing permanent deformations) is more dependent on the elasticity properties of the medium than on the details of the rupture pattern along the fault plane; however, we note the examined magnitude range $5.5 \leq M_w \leq 6.9$ so this statement may not hold for larger ruptures involving more than one asperities or more than one fault planes.

Another important implication of this result (Fig. 4; Fig. 5) is that once a set of PGDs is determined immediately after a strong earthquake, at distances less than 100-km from the epicentre (where broadband seismometers are usually clipped), it may be used to empirically estimate the moment magnitude of the event with an accuracy of 0.3 units.

4. Conclusions

a) We describe and make available a database of GPS horizontal displacements for 11 shallow earthquakes between $M_w=5.5$ and 6.9 around Greece, during the period 1997-2017. We include offsets from GPS sites at near-source to regional distances (2–132 km) with $0.05 \leq \text{PGD} \leq 27.80$ cm or $0.10 \leq \text{PGD-S} \leq 40.58$ cm.

- b) We investigated the magnitude scaling properties of both PGD and PGD-S for these events as a testing for linear attenuation of seismic strain with distance and provide empirical equations relating earthquake magnitude to surface displacement. We find coefficients (see table 3) that are well fit over the magnitude and distance ranges used. The PGD data plot on average around 0.3 magnitude units to the predicted scaling value.
- c) a validation of our estimated (GNSS) magnitude in the case of the 2018 Zakynthos earthquake using the formulas (6) & (7) showed that the magnitude difference with real magnitude (M_w from GCMT) is less than 0.1 magnitude units.
- d) This initial dataset of 64 records may be useful to geologists, seismologists and engineers and we hope to encourage and facilitate the incorporation of GNSS data into ground-motion studies, early-warning systems, and structural monitoring applications.

5. Acknowledgements

The NOANET network was funded by several EU, NATO (Science for Piece) and national research projects from the General Secretariat for Research and Technology of Greece (GSRT). The INGV, NKUA, NTUA, SMARTnet Greece and MIT/UNAVCO has provided geodetic equipment for several stations. GPS Data from the NOANET archive is open and freely available at <http://194.177.194.238:8080/noanetgsac/>. We thank KTIMATOLOGIO, METRICA-SMARTnet GREECE, URANUS, TUTGA, CRL and ETHZ networks for their data. GlobalCMT earthquake data came from <http://globalcmt.org>, and NOA data on earthquake locations are available from <http://bbnet.gein.noa.gr/HL/databases/database>. Data of ASTER GDEM is the property of METI and NASA. Bathymetry data used in figures are from EMODnet Bathymetry Consortium. We acknowledge support of this research by the project “*HELPOS—Hellenic System for Lithosphere Monitoring*” (MIS 5002697).

We thank Diego Melgar, Marco Anzidei, Pierre Briole, Rob Reilinger, Panagiotis Elias, Panagiotis Grigorakakis, Ioannis Kassaras, Chris Pikridas and

Jianghui Geng for discussions and Ricardo Caputo, Iannis Koukouvelas and Panagiotis Psimoulis for comments on the manuscript. We also thank Erietta Vlachou for editorial assistance. P.A was funded by University of Peloponnese and Stavros Niarchos Foundation. This work is part of the MSc thesis of N.A at the National and Kapodistrian University of Athens.

6. References

Atzori S., M. Manunta, G. Fornaro, A. Ganas, S. Salvi, 2008. Postseismic displacement of the 1999 Athens earthquake retrieved by the Differential Interferometry by Synthetic Aperture Radar time series, *Journal of Geophysical Research*, 113, B09309, doi:10.1029/2007JB005504.

Avallone A., P. Briole, A.M. Agatza-Balodimou, H. Billiris, O. Charade, C. Mitsakaki, A. Nercessian, K. Papazissi, D. Paradissis, G. Veis, 2004. Analysis of eleven years of deformation measured by GPS in the Corinth Rift Laboratory area, *C.R. Geoscience*, 336, 301-312.

Avallone A., et al., 2017. Near-source high-rate GPS, strong motion and InSAR observations to image the 2015 Lefkada (Greece) Earthquake rupture history, *Scientific Reports* 7, Article number: 10358, doi:10.1038/s41598-017-10431-w

Argyarakis, P. Ganas, A and Sagiass, N., 2016. The NOANET GSAC (Geodesy Seamless Archive Centers) tool for GNSS data dissemination in SE Europe, *ESC2016-144*.

Bock, Y. and Melgar, D., 2016. Physical applications of GPS geodesy: a review. *Reports on Progress in Physics*, 79(10), p.106801.

Briole, P., P. Elias, I. Parcharidis, C. Bignami, G. Benekos, S. Samsonov, C. Kyriakopoulos, S. Stramondo, N. Chamot-Rooke, M.L. Drakatos, G. Drakatos, 2015. The seismic sequence of January–February 2014 at Cephalonia Island (Greece): constraints from SAR interferometry and GPS, *Geophysical Journal International*, 203, 3, 1528–1540, <https://doi.org/10.1093/gji/ggv353>


Cheloni D., et al. 2014. Coseismic and post-seismic slip of the 2009 L'Aquila (central Italy) Mw 6.3 earthquake and implications for seismic potential along the Campotosto fault from joint inversion of high-precision levelling, InSAR and GPS data, *Tectonophysics*, 622, 168–185, doi:10.1016/j.tecto.2014.03.009.

Chousianitis K., Ganas A., Papanikolaou M., Argyrakis P., Drakatos G. and Makropoulos K., 2013. Time series analysis of the NOANET CGPS stations, *Bulletin of the Geological Society of Greece*, vol. 47 (2), 508-517, <http://dx.doi.org/10.12681/bgsg.11078>

Chousianitis, K., A. Ganas, and C. P. Evangelidis, 2015. Strain and rotation rate patterns of mainland Greece from continuous GPS data and comparison between seismic and geodetic moment release, *J. Geophys. Res. Solid Earth*, 120, 3909–3931.

Chousianitis, K., A. O. Konca, G.-A. Tselentis, G. A. Papadopoulos, and M. Gianniou, 2016. Slip model of the 17 November 2015 Mw = 6.5 Lefkada earthquake from the joint inversion of geodetic and seismic data, *Geophys. Res. Lett.*, 43, doi:10.1002/2016GL069764.

Chousianitis, K., and Konca, A.O., 2018. Coseismic slip distribution of the 12 June 2017 Mw = 6.3 Lesvos earthquake and imparted static stress changes to the neighboring crust. *Journal of Geophysical Research Solid Earth*, 123. <https://doi.org/10.1029/2018JB015950>

Crowell, B. W., D. Melgar, Y. Bock, J. S. Haase, and J. Geng, 2013. Earthquake magnitude scaling using seismogeodetic data, *Geophys. Res. Lett.*, 40, 6089–6094, doi:10.1002/2013GL058391. 

Crowell, B. W., D. A. Schmidt, P. Bodin, J. E. Vidale, J. Gomberg, J. Renate Hartog, V. C. Kress, T. I. Melbourne, M. Santillan, S. E. Minson, and D. G. Jamison, 2016. Demonstration of the Cascadia G-FAST geodetic earthquake early warning system for the Nisqually, Washington, earthquake, *Seismological Research Letters* 87(4), pp.930-943.

Devoti, R. L. Anderlini, M. Anzidei, A. Esposito, A. Galvani, G. Pietrantonio, A. Pisani, F. Riguzzi, V. Sepe, E. Serpelloni, 2012. The coseismic and postseismic deformation of the L'Aquila, 2009 earthquake from repeated GPS measurements. *Italian Journal of Geosciences*; 131 (3): 348–358. doi: <https://doi.org/10.3301/IJG.2012.15>

Estey, L. H. and Meertens, C. M., 1999. TEQC: The Multi-Purpose Toolkit for GPS/GLONASS Data, *GPS Solutions*, 3, 1, 42-49, doi:10.1007/PL00012778.

Ganas, A., G. Drakatos, S. Rontogianni, C. Tsimi, P. Petrou, M. Papanikolaou, P. Argyrakis, K. Boukouras, N. Melis and G. Stavrakakis, 2008. NOANET: the new permanent GPS network for Geodynamics in Greece. *Geophysical Research Abstracts*, Vol. 10, EGU2008-A-04380.

Ganas, A., Serpelloni, E., Drakatos, G., Kolligri, M., Adamis, I., Tsimi, Ch. and Batsi, E., 2009. The Mw 6.4 SW Achaia (Western Greece) Earthquake of 8 June 2008: Seismological, Field, GPS Observations, and Stress Modeling, *Journal of Earthquake Engineering*, 13:8, 1101 — 1124.

Ganas, A., K. Chousianitis, G. Drakatos, M. Papanikolaou, P. Argyrakis, M. Kolligri, P. Petrou, E. Batsi, and C. Tsimi, 2011. NOANET: High-rate GPS Network for Seismology and Geodynamics in Greece. *Geophysical Research Abstracts*, Vol. 13, EGU2011-4840, EGU General Assembly 2011

Ganas, A., K. Chousianitis, M. Papanikolaou, P. Argyrakis, G. Drakatos, K. Makropoulos, 2012. Continuous GPS Velocity Profiles and Baseline Rate Changes in Central and Western Greece: Comparison with Geological Data, In: *Book of Abstracts, 33rd General Assembly of ESC, 19-24 August 2012 Moscow*, p. 125.

Ganas, A., Marinou A, Anastasiou D., Paradissis D., Papazissi K., Tzavaras P., Drakatos G., 2013a. GPS-derived estimates of crustal deformation in the central and north Ionian Sea, Greece: 3-yr results from NOANET continuous network

data. *Journal of Geodynamics*, 67, 62–71.
<http://dx.doi.org/10.1016/j.jog.2012.05.010>

Ganas, A., Chousianitis, K., Batsi, E., Kolligri, M., Agalos, A., Chouliaras, G., & Makropoulos, K., 2013b. The January 2010 Efpalion earthquakes (Gulf of Corinth, Central Greece): earthquake interactions and blind normal faulting. *Journal of Seismology*, 17 (2), 465-484, <http://dx.doi.org/10.1007/s10950-012-9331-6>

Ganas A., Cannavo F., Chousianitis K., Kassaras I., and Drakatos G., 2015. Displacements recorded on continuous GPS stations following the 2014 M6 Cephalonia (Greece) earthquakes: dynamic characteristics and kinematic implications. *Acta Geodyn. Geomater.*, Vol. 12, No. 1 (177), 5–27, 10.13168/AGG.2015.0005.

Ganas, A., Elias, P., Bozionelos, G., Papathanassiou, G., Avallone, A., Papastergios, A., Valkaniotis, S., Parcharidis, I., Briole, P., 2016. Coseismic deformation, field observations and seismic fault of the 17 November 2015 M = 6.5, Lefkada Island, Greece earthquake, *Tectonophysics*, 687, 210-222, <http://dx.doi.org/10.1016/j.tecto.2016.08.012>

Ganas, A., Kourkouli, P., Briole, P., Moshou, A., Elias, P., Parcharidis, I., 2018. Coseismic Displacements from Moderate-Size Earthquakes Mapped by Sentinel-1 Differential Interferometry: The Case of February 2017 Gulpinar Earthquake Sequence (Biga Peninsula, Turkey). *Remote Sens.*, 10, 1089, <http://www.mdpi.com/2072-4292/10/7/1089>

Ganas, A. et al., in review. The July 20, 2017 M6.6 Kos earthquake: seismic and geodetic evidence for an active north-dipping normal fault at the western end of the Gulf of Gökova (SE Aegean Sea).

Geng, T., X. Xie, R. Fang, X. Su, Q. Zhao, G. Liu, H. Li, C. Shi, and J. Liu, 2016. Real-time capture of seismic waves using high-rate multi-GNSS observations: Application to the 2015 Mw 7.8 Nepal earthquake, *Geophys. Res. Lett.*, 43, 161–167, doi:10.1002/2015GL067044.

Geng J., Jiang P., Liu J. 2017. Integrating GPS with GLONASS for high-rate seismogeodesy. *Geophys. Res. Lett.* 44, 3139-3146. doi:10.1002/2017GL072808

Gianniou, M., 2011. Detecting permanent displacements caused by earthquake using data from the HEPOS network, in Proceedings of EUREF 2011 Symposium, May 25–28 2011, Chisinau, Moldova.

Hilla, S., 2004. Plotting pseudorange multipath with respect to satellite azimuth and elevation. *GPS Solutions*, 8: 44. <https://doi.org/10.1007/s10291-004-0086-6>.

Hollenstein, Ch., A. Geiger, H.-G. Kahle, G. Veis, 2006. CGPS time-series and trajectories of crustal motion along the West Hellenic Arc, *Geophysical Journal International*, 164, 1, 182–191, <https://doi.org/10.1111/j.1365-246X.2005.02804.x>

Hollenstein, Ch., M. D. Müller, A. Geiger, H.-G. Kahle, 2008. GPS-Derived Coseismic Displacements Associated with the 2001 Skyros and 2003 Lefkada Earthquakes in Greece. *Bulletin of the Seismological Society of America*; 98 (1): 149–161. doi: <https://doi.org/10.1785/0120060259>

Howell, A., K. Palamartchouk, X. Papanikolaou, D. Paradissis, C. Raptakis, A. Copley, P. England, J. Jackson, 2017. The 2008 Methoni earthquake sequence: the relationship between the earthquake cycle on the subduction interface and coastal uplift in SW Greece, *Geophysical J. International*, 208, 1592–1610, <https://doi.org/10.1093/gji/ggw462>

Hreinsdottir, S., T. Arnadottir, J. Decriem, H. Geirsson, A. Tryggvason, R. A. Bennett, and P. LaFemina, 2009. A complex earthquake sequence captured by the continuous GPS network in SW Iceland, *Geophys. Res. Lett.*, 36, L12309, doi:10.1029/2009GL038391.

Huang M-H, D. Dreger, R. Bürgmann, S-H Yoo, M. Hashimoto, 2013. Joint inversion of seismic and geodetic data for the source of the 2010 March 4, Mw 6.3 Jia-Shian, SW Taiwan, earthquake, *Geophysical Journal International*, 193, 3, 1608–1626, <https://doi.org/10.1093/gji/ggt058>

Ilieva, M., P. Briole, A. Ganas, D. Dimitrov, P. Elias, A. Mouratidis, R. Charara, 2016. Fault plane modelling of the 2003 August 14 Lefkada Island (Greece) earthquake based on the analysis of ENVISAT SAR interferograms, *Tectonophysics*, 693, 47-65, <http://dx.doi.org/10.1016/j.tecto.2016.10.021>

Johanson, I., and R. Bürgmann, 2010. Coseismic and postseismic slip from the 2003 San Simeon earthquake and their effects on backthrust slip and the 2004 Parkfield earthquake, *J. Geophys. Res.*, 115(B7), B07411, doi:10.1029/2009JB006599.

Karastathis, V. K., Mouzakiotis, E., Ganas, A., and Papadopoulos, G. A., 2015. High-precision relocation of seismic sequences above a dipping Moho: the case of the January–February 2014 seismic sequence on Cephalonia island (Greece), *Solid Earth*, 6, 173-184, doi:10.5194/se-6-173-2015.

King, G. C. P., Stein, R. S., & Rundle, J. B., 1988. The growth of geological structures by repeated earthquakes 1. Conceptual framework. *Journal of Geophysical Research*, 93(B11), 13,307–13,318. <https://doi.org/10.1029/JB093iB11p13307>

Kiratzi, A., E. Tsakiroudi, C. Benetatos, G. Karakaisis, 2016. The 24 May 2014 (Mw6.8) earthquake (North Aegean Trough): spatiotemporal evolution, source and slip model from teleseismic data. *Phys. Chem. Earth*, 95, p. 85e100, 10.1016/j.pce.2016.08.003.

Marinou, A., A. Ganas, K. Papazissi, D. Paradissis, 2015. Strain patterns along the Kaparelli–Asopos rift (central Greece) from campaign GPS data. *Annals of Geophysics*, 58, 2, S0219 <http://www.annalsofgeophysics.eu/index.php/annals/article/view/6418>

Marshall, J. 2002. Creating and viewing skyplots. *GPS Solutions*, 6: 118.
<https://doi.org/10.1007/s10291-002-0017-3>

Melgar, D., B.W. Crowell, J. Geng, R.M. Allen, Y. Bock, S. Riquelme, E.M. Hill, M. Protti, and A. Ganas, 2015. Earthquake magnitude calculation without saturation from the scaling of peak ground displacement, *Geophysical Research Letters*, 42, <http://onlinelibrary.wiley.com/doi/10.1002/2015GL064278/full>

Melgar, D., A. Ganas, J. Geng, C. Liang, E. J. Fielding, and I. Kassaras, 2017. Source characteristics of the 2015 Mw6.5 Lefkada, Greece, strike-slip earthquake, *J. Geophys. Res. Solid Earth*, 122, <http://dx.doi.org/10.1002/2016JB013452>

Moschas, F., and S. Stiros, 2011. Measurement of the dynamic displacements and of the modal frequencies of a short-span pedestrian bridge using GPS and an accelerometer, *Engineering Structures*, 33, 1, 10-17, <https://doi.org/10.1016/j.engstruct.2010.09.013> .

Moschas F, Stiros SC, 2014. Three-dimensional dynamic deflections and natural frequencies of a stiff footbridge based on measurements of collocated sensors. *Struct Control Health Monit* 21(1):23–42. doi: 10.1002/stc.1547.

Murray, J. R., B. W. Crowell, R. Grapenthin, K. Hodgkinson, J. O. Langbein, T. Melbourne, D. Melgar, S. E. Minson, D. A. Schmidt, 2018. Development of a Geodetic Component for the U.S. West Coast Earthquake Early Warning System. *Seismological Research Letters*, 89, (6), 2322-2336, doi: <https://doi.org/10.1785/0220180162>

Nappi, R., Gaudiosi, G., Alessio, G. et al., 2017. The environmental effects of the 1743 Salento earthquake (Apulia, southern Italy): a contribution to seismic hazard assessment of the Salento Peninsula. *Nat Hazards*, 86 (Suppl. 2): 295. <https://doi.org/10.1007/s11069-016-2548-x>

Pearce, F. D., Rondenay, S., Sachpazi, M., Charalampakis, M. and Royden, L.H., 2012. Seismic investigation of the transition from continental to oceanic

subduction along the western Hellenic Subduction Zone. *Journal of Geophysical Research*, 117, B07306. DOI: 10.1029/2011JB009023

Reilinger R., et al., 2006. GPS constraints on continental deformation in the Africa-Arabia-Eurasia continental collision zone and implications for the dynamics of plate interactions, *J. Geophys. Res.*, 111, B05411, doi:10.1029/2005JB004051.

Rontogianni, S. 2010. Comparison of geodetic and seismic strain rates in Greece by using a uniform processing approach to campaign GPS measurements over the interval 1994–2000, *J. Geodyn.*, 50, 381–399, doi:10.1016/j.jog.2010.04.008

Ruhl, C. J., D. Melgar, R. Grapenthin, and R. M. Allen, 2017. The value of real-time GNSS to earthquake early warning, *Geophys. Res. Lett.*, 44, 8311–8319, doi:10.1002/2017GL074502.

Ruhl, C. J, D. Melgar, J. Geng, D.E Goldberg, B.W Crowell, R.M Allen, Y. Bock, S. Barrientos, S. Riquelme, JC Baez, E. Cabral-Cano, X. Pérez-Campos, E.M Hill, M. Protti, A. Ganas, M. Ruiz, P. Mothes, P. Jarrín, J-M. Nocquet, J.-P. Avouac, E. D'Anastasio, 2018. A Global Database of Strong-Motion Displacement GNSS Recordings and an Example Application to PGD Scaling, *Seismological Research Letters*, <https://doi.org/10.1785/0220180177>

Sakkas V, Lagios E. 2017. Ground Deformation Effects from the ~M6 Earthquakes (2014-2015) on Cephalonia-Ithaca Islands (W. Greece) deduced by GPS Observations, *Acta Geophysica*, doi.: 10.1007/s11600-017-0017-x.

Saltogianni, V., M. Gianniou, T. Taymaz, S. Yolsal-Çevikbilen, and S. Stiros, 2015. Fault slip source models for the 2014 Mw 6.9 Samothraki-Gökçeada earthquake (North Aegean Trough) combining geodetic and seismological observations, *J. Geophys. Res. Solid Earth*, 120, 8610–8622, doi: 10.1002/2015JB012052.

Serpetsidaki, A., Elias P., Ilieva M., Bernard P., Briole, P., Deschamps, A., Lambotte, S, Lyon-Caen, H., Sokos, E and Tselentis, A. 2014. New constraints

from seismology and geodesy on the $M_w = 6.4$ 2008 Movri (Greece) earthquake: Evidence for a growing strike-slip fault system. *Geophysical Journal International*, 198,1373-1386. 10.1093/gji/ggu212.

Tiryakioğlu, İ., B. Aktuğ, C. Ö. Yiğit, H. H. Yavaşoğlu, H. Sözbilir, Ç. Özkaymak, F. Poyraz, E. Taneli, F. Bulut, A. Doğru & H. Özener, 2018. Slip distribution and source parameters of the 20 July 2017 Bodrum-Kos earthquake ($M_w 6.6$) from GPS observations, *Geodinamica Acta*, 30:1, 1-14, DOI: 10.1080/09853111.2017.1408264

Supplementary material

Figure S1. Number of earthquake recordings per GNSS station. Data are reported in Table S1.

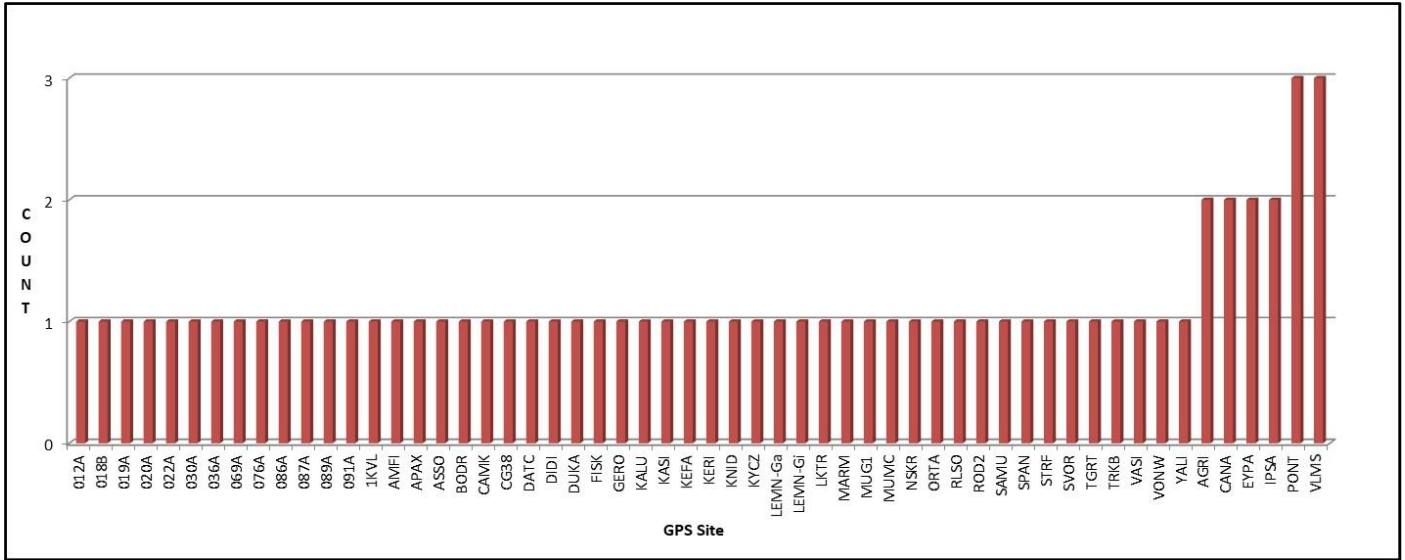


Table S1. GPS Displacement data for Greek earthquakes, period 1997-2017. Data sources (column REF) are: (1) Hollenstein et al., 2006 (2) Hollenstein et al., 2008 (3) Ganas et al., 2009 (4) Gianniou, 2011 (5) Ganas, et al., 2013 (6) Ganas et al., 2015 (7) Ganas et al., 2014, unpublished report http://www.gein.noa.gr/Documents/pdf/May_24_2014_GPS_report.pdf (8) Saltogianni et al., 2015 (9) Ganas et al., 2016 and (10) Ganas et al. in review (including data from Tiryakioglou et al., 2017). PGD and PGD-S are calculated according to equations (1) and (2), respectively.

Offset No	Event No	Date	Mw (GCMT)	GPS Site	Distance to Hypocentre (km)	PGD-S (cm)	PGD (cm)	REF
1	1	19971118	6.6	STRF	39.686	11.76	6.45	1
2	1	19971118	6.6	KERI	24.201	2.02	1.40	1
3	2	20010726	6.4	NSKR	31.119	7.45	4.15	2
4	2	20010726	6.4	CG38	51.637	3.68	2.60	2
5	3	20030814	6.2	APAX	48.821	0.78	0.55	2
6	3	20030814	6.2	VONW	21.063	3.11	2.20	2
7	3	20030814	6.2	AMFI	46.110	0.50	0.35	2
8	3	20030814	6.2	1KVL	8.164	7.21	4.50	2
9	3	20030814	6.2	VASI	26.338	4.04	2.30	2
10	3	20030814	6.2	DUKA	31.559	5.59	3.95	2
11	3	20030814	6.2	FISK	42.065	3.45	2.15	2
12	3	20030814	6.2	ASSO	52.143	2.94	1.85	2
13	3	20030814	6.2	GERO	77.079	0.20	0.10	2
14	3	20030814	6.2	LKTR	78.774	0.22	0.15	2
15	4	20080608	6.4	RLSO	22.162	0.70	0.35	3
16	4	20080608	6.4	030A	26.241	0.80	0.55	4
17	4	20080608	6.4	012A	51.264	0.70	0.50	4
18	5	20100118	5.5	EYPA	9.401	0.68	0.48	5
19	6	20100122	5.4	EYPA	5.662	0.37	0.24	5
20	7	20140126	6.1	VLMS	20.239	1.17	0.79	6
21	7	20140126	6.1	PONT	49.535	0.25	0.15	6
22	7	20140126	6.1	AGRI	49.094	0.11	0.08	6
23	7	20140126	6.1	SVOR	20.331	1.30	0.85	6
24	7	20140126	6.1	KEFA	16.701	5.32	3.60	6
25	8	20140203	6.0	VLMS	18.057	1.79	1.23	6
26	8	20140203	6.0	PONT	40.953	0.27	0.16	6
27	8	20140203	6.0	AGRI	93.779	0.13	0.09	6
28	9	20140524	6.9	CANA	89.490	3.04	2.08	7
29	9	20140524	6.9	IPSA	109.030	1.93	1.31	7
30	9	20140524	6.9	LEMN-Gi	49.521	5.25	3.51	7
31	9	20140524	6.9	LEMN-Ga	49.521	4.95	3.24	7
32	9	20140524	6.9	018B	26.924	10.20	6.45	8
33	9	20140524	6.9	089A	47.820	5.69	3.75	8
34	9	20140524	6.9	019A	70.655	1.94	1.37	8

35	9	20140524	6.9	036A	86.966	1.08	0.74	8
36	9	20140524	6.9	076A	127.601	0.34	0.24	8
37	9	20140524	6.9	020A	137.857	0.89	0.63	8
38	9	20140524	6.9	022A	118.047	1.02	0.71	8
39	9	20140524	6.9	069A	90.536	0.92	0.60	8
40	9	20140524	6.9	091A	131.284	0.41	0.24	8
41	9	20140524	6.9	CANA	89.490	3.04	2.05	8
42	9	20140524	6.9	IPSA	109.030	2.00	1.41	8
43	10	20151117	6.5	KASI	132.204	0.10	0.05	9
44	10	20151117	6.5	SPAN	16.717	9.32	6.55	9
45	10	20151117	6.5	VLSM	56.279	0.70	0.35	9
46	10	20151117	6.5	PONT	11.500	40.58	27.80	9
47	11	20170720	6.6	086A	33.960	1.35	0.95	10
48	11	20170720	6.6	087A	82.852	0.58	0.40	10
49	11	20170720	6.6	BODR	12.351	16.45	9.90	10
50	11	20170720	6.6	CAMK	44.562	2.81	1.50	10
51	11	20170720	6.6	DATC	36.144	3.35	2.10	10
52	11	20170720	6.6	DIDI	49.861	1.96	1.20	10
53	11	20170720	6.6	KALU	44.219	0.71	0.40	10
54	11	20170720	6.6	KNID	32.099	5.39	3.50	10
55	11	20170720	6.6	KYCZ	110.402	1.34	0.90	10
56	11	20170720	6.6	MARM	50.907	0.63	0.40	10
57	11	20170720	6.6	MUG1	85.973	0.40	0.20	10
58	11	20170720	6.6	MUMC	27.014	7.27	4.60	10
59	11	20170720	6.6	ORTA	16.612	10.73	6.95	10
60	11	20170720	6.6	ROD2	112.609	0.63	0.40	10
61	11	20170720	6.6	SAMU	99.015	0.91	0.50	10
62	11	20170720	6.6	TGRT	20.186	2.66	1.70	10
63	11	20170720	6.6	TRKB	22.811	6.96	4.50	10
64	11	20170720	6.6	YALI	12.795	15.32	8.00	10

Text S1.

The **A**, **B**, **C** coefficients we are calculating can be assumed as random variables. Using 6-fold cross validated lasso regression in MATLAB we calculated 100 values for each coefficient for 100 different λ .

We put the values in a single matrix **M** which we can consider as a random vector. Each column represents a vector with elements the 100 values of the coefficient **A**, **B**, or **C**.

We would need the 3x3 covariance matrix to fully characterize the variation of the coefficients. The covariance matrix represents the variance of **A**, **B** and **C** and the covariance between **A** and **B**, **B** and **C** and **A** and **C**.

The variance $\text{Var}(\mathbf{X})$ and covariance $\text{Cov}(\mathbf{X}, \mathbf{Y})$ are calculated as follows:

$$\text{Var}(\mathbf{X}) = \sum_i (\mathbf{X}_{\text{mean}} - X_i)^2 = \sum_i x_i^2 / N$$

$$\text{Cov}(\mathbf{X}, \mathbf{Y}) = \sum_i (\mathbf{X}_{\text{mean}} - X_i)(\mathbf{Y}_{\text{mean}} - Y_i) = \sum_i x_i y_i / N$$

Where X_i and Y_i are the i -th elements of the **X** and **Y** vectors that represent the sets of N random values for the **X** and **Y** random variables, X_{mean} and Y_{mean} represent the mean values of **X** and **Y** and $x_i = (X_{\text{mean}} - X_i)$, $y_i = (Y_{\text{mean}} - Y_i)$.

Using MATLAB we calculated the covariance matrix for the coefficients **A**, **B** and **C** that lasso regression returned and we obtained two matrices, one for the PGD-approach and one for the PGD-S approach.

$$\mathbf{M} = \begin{matrix} & \text{Var}(\mathbf{A}) & \text{Cov}(\mathbf{B}, \mathbf{A}) & \text{Cov}(\mathbf{C}, \mathbf{A}) \\ \text{Cov}(\mathbf{A}, \mathbf{B}) & \text{Var}(\mathbf{B}) & & \text{Cov}(\mathbf{C}, \mathbf{B}) \\ \text{Cov}(\mathbf{A}, \mathbf{C}) & \text{Cov}(\mathbf{B}, \mathbf{C}) & \text{Var}(\mathbf{C}) & \end{matrix}$$

Our results are presented in the following tables:

PGD	A	B	C
A	4.2659	-0.8515	0.1188
B	-0.8515	0.1700	-0.0237
C	0.1188	-0.0237	0.0033

Table 4. The covariance matrix for the **A**, **B**, **C** coefficients calculated using PGD.

PGD-S	A	B	C
A	4.2337	-0.845	0.1178
B	-0.8450	0.1687	-0.0235
C	0.1178	-0.0235	0.0033

Table 5. The covariance matrix for the **A**, **B**, **C** coefficients calculated using PGD-S.